PROCEEDINGS OF SCIENCE

Towards Quantum Monte Carlo Simulations at non-zero Baryon and Isospin Density in the Strong Coupling Regime

Pratitee Pattanaik[a] **and Wolfgang Unger**[a,*]

[a] *Fakultät für Physik, Universität Bielefeld,*
Bielefeld, Germany

E-mail: pratiteep@physik.uni-bielefeld.de, wunger@physik.uni-bielefeld.de

The Hamiltonian formulation of Lattice QCD with staggered fermions in the strong coupling limit has no sign problem at non-zero baryon density and allows for Quantum Monte Carlo simulations. We have extended this formalism to two flavors, and after a resummation, there is no sign problem both for non-zero baryon and isospin chemical potential. We report on recent progress on the implementation of the Quantum Monte Carlo simulations.

The 39th International Symposium on Lattice Field Theory (Lattice2022),
8-13 August, 2022
Bonn, Germany

*Speaker

PoS(LATTICE2022)162

1. Introduction

Lattice QCD with staggered fermions in the strong coupling limit has been studied both via Monte Carlo [1–3] and mean field theory [4, 5] in the last decades. Whereas the mean field approach is based on a $1/d$ expansion, the formulation suitable for Monte Carlo is a dual representation where the degrees degrees of freedom are color singlets, such as mesons and baryons. It is obtained by integrating out the gauge fields first, after that the Grassmann variables. This formulation has no fermion determinant, but admits a world-line representation. In this dual representation, the finite density sign problem is much milder, as the sign only depends on the the geometry of baryonic world-lines. This effective theory of lattice QCD can be very efficiently simulated by the worm algorithm [3]. It has been extended via the strong coupling expansion to non-zero values of the inverse gauge coupling $\beta = \frac{2N_c}{g^2}$ [6].

The main motivation for lattice QCD in the strong coupling regime is that the finite density sign problem is mild enough to study the full μ_B-T phase diagram. This is still possible if the inverse gauge coupling β is not too large [7, 8]. The drawback of the dual representation is that the sign problem is gradually re-introduced as the lattice gets finer, hence the continuum limit is out of reach. The phase diagram in the strong coupling regime features a critical endpoint at finite quark mass (tricritical in the chiral limit), which for moderate quark is located at values much larger than $\mu_{B,c}/T_c > 3$ [9]. Whether the chiral critical point still exists in the continuum limit is unknown.

Even though the continuum limit $a \to 0$ is out of reach in the dual representation, we have studied the continuous time limit $a_t \to 0$, which results in a Quantum Hamiltonian formulation of lattice QCD. Anisotropic lattices with $\xi = a/a_t > 1$ are necessary because the spatial lattice spacing a is fixed for fixed β, and introducing a bare anisotropy γ is the only way to continuously vary the temperature $aT = \xi/N_\tau$. At fixed bare temperature aT, the limits $a_t \to 0$ and $N_t \to \infty$ are taken simultaneously [10]. The continuous time limit has many advantages over the formulation on 3+1 dimensional lattice with discrete temporal extent N_τ:

- The sign problem is completely absent as baryons become static for $a_t \to 0$.
- Ambiguities on the phase boundary present for finite N_τ are remediated.
- The dual degrees of freedom can be mapped onto pion occupation numbers.
- A quantum Monte Carlo algorithm (continuous time worm algorithm) can be used to directly sample the continuous time partition function.
- Continuous time correlation function can be used to determine the hadron masses.

The Hamiltonian formulation of lattice QCD has been discussed in detail in [11] in the strong coupling limit for $N_f = 1$. In contrast to Hamiltonian formulations in the early days of lattice QCD [12] this formulation is based on the continuous time limit of the dual representation. Whereas in meanfield theory also the extension from $N_f = 1$ flavor of staggered fermions to $N_f = 2$ is straight forward [5, 13], the $N_f = 2$ dual formulation is much more involved. As explained in [14], the list of color singlet invariants is much larger, and Grassmann integration yields contractions that introduce a severe sign problem also in the mesonic sector. However, it was also found that in the continuous time limit, the sign problem is again absent. Hence a Quantum Hamiltonian formulation for $N_f = 2$ strong coupling lattice QCD could be found that can be studied via Quantum Monte Carlo. This allows to study various phenomena that are not present in the $N_f = 1$ formulation:

- Simulations at both non-zero baryon and isospin density are possible, hence the phase diagram in the $\mu_B - \mu_I - T$ can be determined
- This will also allow to study the relation between pion condensation and the nuclear phase.
- Nuclear interactions that are purely entropic for $N_f = 1$ are modified by pion exchange between nucleons.

In this prodeedings, we will report on the progress concerning the Quantum Monte Carlo algorithm for the $N_f = 2$ Quantum Hamiltonian

2. Hamiltonian formulation in the strong coupling limit for $N_f = 2$

While it is possible to derive at a Hamiltonian formulation for gauge group SU(3) for any number of flavors, for definiteness we will here restrict to the formulation for $N_f = 2$ in the chiral limit. It should be note that the number of hadronic states quickly grows with the number of flavors, the dimension d of the local Hilbert space $\mathbb{H}_\mathfrak{h}$ is $d = 6$ for $N_f = 1$, $d = 92$ for $N_f = 2$ and $d = 2074$ for $N_f = 3$. The full Hilbert space has thus dimension $D = d^\Omega$ with $\Omega = N_s^3$ the spatial lattice volume. To refine the 92 states for $N_f = 2$ further in terms of baryon and isosopin number and meson occupation numbers, the 1-link integral is expressed via the following invariants [14]:

$$\mathcal{J}(\mathcal{M}, \mathcal{M}^\dagger) = \int_{\mathrm{SU}(3)} dU e^{\mathrm{tr}[U\mathcal{M}^\dagger + U^\dagger \mathcal{M}]} = \sum_{B=-2}^{2} \sum_{n_1,n_2,n_3} C_{B,n_1,n_2,n_3} \frac{E^B}{|B|!} \prod_{i=1}^{3} \frac{X_i^{n_i}}{n_i!}, \quad E = \begin{cases} \det \mathcal{M} & B > 0 \\ 1 & B = 0 \\ \det \mathcal{M}^\dagger & B < 0 \end{cases}$$

$$\begin{aligned}
(\mathcal{M})_{ij} &= \bar{\chi}_i^\alpha(x)\chi_i^\alpha(y), \qquad (\mathcal{M}^\dagger)_{kl} = \chi_k^\beta(y)\bar{\chi}_l^\beta(x), \quad (M_x M_y)^n = (-1)^{n+1}(\mathcal{M}\mathcal{M}^\dagger)^n \\
X_1 &= \mathrm{Tr}[M_x M_y] = M_U + M_D + M_{\pi^+} + M_{\pi^-}, \\
X_2 &= X_1^2 - D_2, \quad X_3 = X_1^3 - 2X_1 D_2, \\
D_2 &= \det[M_x M_y] = M_U M_D + M_{\pi^+} M_{\pi^-} - M^{(2)}_{\pi^+\pi^-,UD} - M^{(2)}_{UD,\pi^+\pi^-} \\
\det \mathcal{M} &= B_{uuu} + B_{uud} + B_{udd} + B_{ddd}, \quad \det \mathcal{M}^\dagger = \bar{B}_{uuu} + \bar{B}_{uud} + \bar{B}_{udd} + \bar{B}_{ddd}
\end{aligned} \tag{1}$$

with C_{B,n_1,n_2,n_3} combinatorial factors that are derived from [15], but expressed in a more suitable basis, in particular expressend in the $N_f = 2$ determinants E and D_2. The M_Q are meson hoppings between nearest neighbor sites $\langle x, y\rangle$, the B_{fgh} are baryons hopping from x to y and $\bar{B}_{fgh}$ anti-baryons hopping from y to x. After Grassmann integration, negative weights occur within the invariant X_2, X_3 due to non-trivial Wick contractions from D_2. However, in the continuous time limit, only single meson exchange survives and $M^{(2)}_{\pi^+\pi^-,UD}$, $M^{(2)}_{UD,\pi^+\pi^-}$ can only appear in temporal direction. Without any resummations, there would be 286 possible states when considering all combinations of invariants from the X_i and E that survive after Grassmann integration. However, upon diagonalization of the transfer matrix from one set of states to another set, many states become resummed and only 92 distinct states survive. An example of such a tranfer matrix for $B = 0$, $I = 0$ is the square matrix which maps the states $\vec{e}_1 = |M_U M_D\rangle$, $\vec{e}_2 = |M_{\pi^+} M_{\pi^-}\rangle$, $\vec{e}_3 = |M^{(2)}_{\pi^+\pi^-,UD}\rangle$ and $\vec{e}_4 = |M^{(2)}_{UD,\pi^+\pi^-}\rangle$ onto each other:

$$\Pi = \begin{pmatrix} \frac{9}{8} & -\frac{3}{8} & \frac{3\sqrt{3}}{8} & -\frac{\sqrt{3}}{8} \\ -\frac{3}{8} & \frac{9}{8} & -\frac{\sqrt{3}}{3} & \frac{3\sqrt{3}}{8} \\ -\frac{\sqrt{3}}{8} & \frac{3\sqrt{3}}{8} & -\frac{1}{8} & \frac{3}{8} \\ -\frac{3\sqrt{3}}{8} & -\frac{\sqrt{3}}{8} & \frac{3}{8} & -\frac{1}{8} \end{pmatrix}. \tag{2}$$

This matrix is a projector, has trace 2, and upon diagonlization, two linear combinations have eigenvalue $\lambda = 0$ and can be disregarded, whereas the other two linear combinations have eigenvalue $\lambda = 1$, which are the distinct states:

$$\begin{aligned} |\pi_1^2\rangle &= \sqrt{3}|M_U M_D\rangle + |M^{(2)}_{UD,\pi^+\pi^-}\rangle \\ |\pi_2^2\rangle &= \sqrt{3}|M_{\pi^+} M_{\pi^-}\rangle + |M^{(2)}_{\pi^+\pi^-,UD}\rangle \end{aligned} \tag{3}$$

Also all other linear combinations that result from diagonalization have eigenvalues $\lambda = 1$, few of them two-fold-degenerated, and all results in positive weights. Hence, the sign problem is absent. In Tab. 1 the 92 quantum states are listed in terms of the the quantum numbers: baryon number B, isospin number I and, number of mesons $\mathfrak{m}$. Those quantum numbers are not yet sufficient to distinguish all 92 states.

However, as we are restricted to the chiral limit, a conservation law for each of the pion currents $\pi_U, \pi_D, \pi_+, \pi_-$ holds. The role of spatial dimers at a bond location $\langle x, y\rangle$ is to transfer pion charge from one site x to site y. Due to the even-odd ordering for staggered fermions, such dimers can be consistently oriented from an emission site x to an absorption site y. As a consequence, if a quantum number $\mathfrak{m}_Q(x)$ is raised/lowered by a spatial dimer, then at the site connected by the spatial meson hopping M_Q the quantum number is lowered/raised. With those interactions derived from a high temperature series, the resulting partition sum can be expressed in terms of a Hamiltonian that is composed of mesonic annihilation and creation operators $\hat{J}^\pm_Q$:

$$\begin{aligned} Z_{\rm CT}(\mathcal{T}, \mu_{\mathcal{B}}, \mu_{\mathcal{I}}, \Omega) &= \mathrm{Tr}_{\mathfrak{h}^\Omega}\left[e^{(\hat{\mathcal{H}} + \hat{\mathcal{N}}_B \mu_{\mathcal{B}} + \hat{\mathcal{N}}_I \mu_{\mathcal{I}})/\mathcal{T}}\right] \qquad \mathfrak{h} \in \mathbb{H}_{\mathfrak{h}} \\ \hat{\mathcal{H}}_I &= \frac{1}{2} \sum_{\langle \vec{x}, \vec{y}\rangle} \sum_{Q_i \in \{\pi^+, \pi^-, \pi_U, \pi_D\}} \left(\hat{J}^+_{Q_i,\vec{x}} \hat{J}^-_{Q_i,\vec{y}} + \hat{J}^-_{Q_i,\vec{x}} \hat{J}^+_{Q_i,\vec{y}}\right) \\ \hat{\mathcal{N}}_B &= \mathrm{diag}(-2, -1, \ldots 1, 2), \qquad \hat{\mathcal{N}}_I = \mathrm{diag}\left(0, -\frac{3}{2}, \ldots \frac{3}{2}, 0\right) \end{aligned}$$

where the matrices per spatial site, $\hat{J}^+_{Q_i}$, $\hat{J}^-_{Q_i}$, $\hat{\mathcal{N}}_B$ and $\hat{\mathcal{N}}_I$ are 92×92 - dimensional and the tensor product over all spatial sites Ω is implied. The 92-dimensional local Hilbert states $\mathbb{H}_{\mathfrak{h}}$ For the transition $\mathfrak{h}_1 \mapsto \mathfrak{h}_2$, the matrix elements $\langle \mathfrak{h}_1|Q_i|\mathfrak{h}_2\rangle$ of $\hat{J}^\pm_{Q_i}$ are determined from Grassmann integration and diagonalization, only those matrix elements are non-zero which are consistent with current conservation of all Q_i.

Since meson occupation numbers are not just bounded from below, but also from above due to the Grassmannian nature of the underlying quarks, they fulfill an algebra that exhibits a particle-hole

B	I	$\mathfrak{s} = \mathfrak{m} - \frac{3}{2}(2-\lvert B\rvert)$													Σ
		-3	$-\frac{5}{2}$	-2	$-\frac{3}{2}$	-1	$-\frac{1}{2}$	0	$+\frac{1}{2}$	$+1$	$+\frac{3}{2}$	$+2$	$+\frac{5}{2}$	$+3$	
-2	0							1							1
-1	$-\frac{3}{2}$				1		1		1		1				4
-1	$-\frac{1}{2}$				1		2		2		1				6
-1	$+\frac{1}{2}$				1		2		2		1				6
-1	$+\frac{3}{2}$				1		1		1		1				4
0	-3							1							1
0	-2					1		2		1					4
0	-1			1		2		4		2		1			10
0	0	1		2		4		6		4		2		1	20
0	-1			1		2		4		2		1			10
0	-2					1		2		1					4
0	-3							1							1
1	$-\frac{3}{2}$				1		1		1		1				4
1	$-\frac{1}{2}$				1		2		2		1				6
1	$+\frac{1}{2}$				1		2		2		1				6
1	$+\frac{3}{2}$				1		1		1		1				4
2	0							1							1
Σ		1	0	4	8	10	12	22	12	10	8	4	0	1	92

Table 1: All 92 possible quantum states on a single site for the $N_f = 2$ Hamiltonian formulation with SU(3) gauge group. The number of states are given for the sectors specified baryon number B and isospin number I, and symmetrized meson occupation number $\mathfrak{s} = \mathfrak{m} - \frac{N_c}{2}(N_f - |B|)$. Note the mesonic particle-hole symmetry $\mathfrak{s} \leftrightarrow -\mathfrak{s}$ which corresponds to the shift symmetry by a_τ.

symmetry, the meson occupation numbers can be mapped onto a symmetrized occupation number $\mathfrak{s} = \mathfrak{m} - \frac{3}{2}(2-|B|)$. On discrete lattices, particles are mapped to anti-particles by a shift of a_t due to the even-odd ordering of staggered fermions, but this relation also survives in the continuous time limit $a_t \to 0$.

The matrices $\hat{J}^{\pm}_{Q_i}$ hence span a $\frac{3}{2}(2-|B|)$-dimensional representation of a Lie algebra, as illustrated in Fig. 1. The arrows in different colors correspond to the raising ladder operators $\hat{J}^{+}_{Q_i}$, each of the four colors generates a specific meson. The representation for $\hat{J}^{\pm}_{\pi_U}$ and $\hat{J}^{\pm}_{\pi_D}$ is a direct product representation, likewise $\hat{J}^{\pm}_{\pi^+}$ and $\hat{J}^{\pm}_{\pi^-}$, but both Lie algebras meet in various states, as they are not distinguished on the quark level, e.g.

$$|\pi_+\pi_-\rangle = |\pi_U\pi_D\rangle, \qquad |B_{uuu}\pi_D\rangle = |B_{uud}\pi_-\rangle, \qquad |B_{uuu}B_{ddd}\rangle = |B_{uud}B_{udd}\rangle.$$

Those states in Fig. 1that are twofold degenerated as for $|m_1^2\rangle$, $|m_2^2\rangle$ in Eq. (3) are highlighted in bold: 5 such states for $B=0$ and 2 states degenerate for $B=1$ and also for $B=-1$. We label all 92 hadronic states of the local Hilbert space by their quark content in lexicographical order: first order by B, I and $\mathfrak{m}$ and then by the sequence of occupations in $\bar{u}$, u, $\bar{d}$, d. However, the quark content is not sufficient to distinguish those 9 states that are two-fold degenerate: here we introduce an additional index $i \in \{0, 1\}$ that is required by the QMC algorithm as explained in the next section.

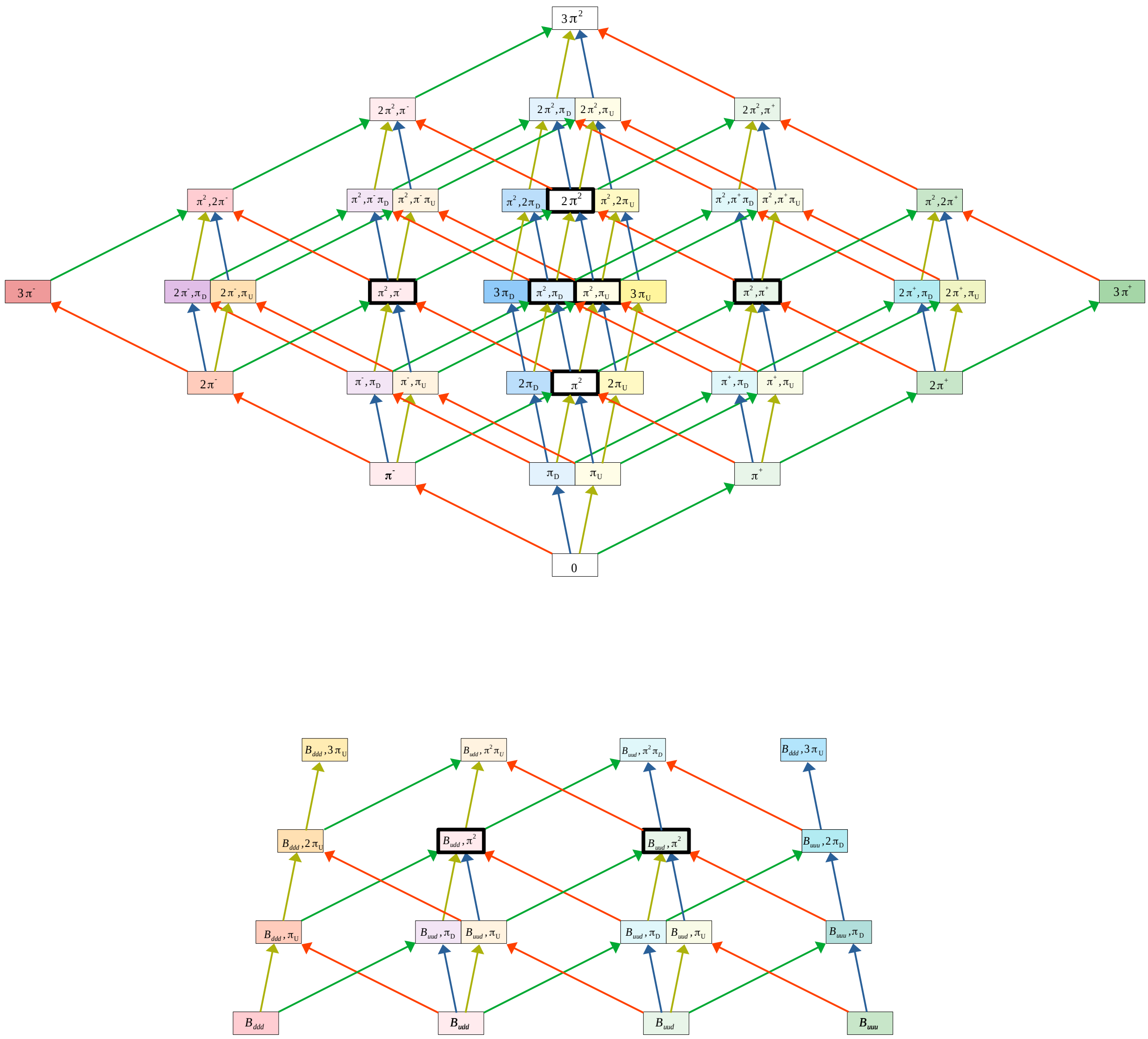

Figure 1: Depiction of how ladder operators connect the various hadronic states, for $B = 0$ (top) and $B = 1$ (bottom). The bold boxes are two-fold degenerated, see Eq. (3). The red arrows correspond to $\hat{J}^+_{\pi^-}$, the green arrows to $\hat{J}^+_{\pi^+}$, the blue arrows to $\hat{J}^+_{\pi_D}$ and the yellow arrows to $\hat{J}^+_{\pi_U}$. In the weight diagrams it can be seen that both the root system spanned by $\hat{J}^+_{\pi^+}$,$\hat{J}^+_{\pi^-}$ is orthogonal, and the root system spanned by $\hat{J}^+_{\pi_U}$,$J^+_{\pi_D}$ is orthogonal, both are direct product of two $N_c + 1$-dimensional representations, however, both system mix and cannot be treated independently. The horizontal axis label isospin, the vertical axis labels meson occupation numbers.

The ladder operators fulfill the following identities:

$$[\hat{J}^+_{Q_i}, \hat{J}^-_{Q_i}] = \begin{pmatrix} -1 & 0 & 0 & 0 \\ 0 & -1/3 & 0 & 0 \\ 0 & 0 & 1/3 & 0 \\ 0 & 0 & 0 & 1 \end{pmatrix} = \frac{2}{N_c}\hat{J}^{(3)}_{Q_i}, \qquad [\hat{J}^+_{Q_i}, \hat{J}^-_{Q_j}] = 0 \quad \text{for} \quad i \neq j. \tag{4}$$

,

Examples of matrix elements of $\hat{J}^+_{Q_i}$ (with $\pi_1 = \pi_U$, $\pi_2 = \pi_D$, $\pi_3 = \pi^+$ and $\pi_4 = \pi^-$) are:

$$\langle 0|\hat{J}^+_{Q_i}|\pi_i\rangle = 1, \quad \langle \pi_i|\hat{J}^+_{Q_i}|2\pi_i\rangle = \frac{2}{\sqrt{3}}, \quad \langle 2\pi_i|\hat{J}^+_{Q_i}|3\pi_i\rangle = 1 \quad \text{for} \quad i \in \{1,2,3,4\}$$

$$\langle \pi_i|\hat{J}^+_{Q_j}|\pi_i\pi_j\rangle = 1 \quad \text{for} \quad i \neq j$$

$$\langle \pi_U|\hat{J}^+_{\pi_D}|\pi_1^2\rangle = \langle \pi_D|J^+_{\pi_U}|\pi_1^2\rangle = \frac{\sqrt{6}}{4}, \quad \langle \pi_U|J^+_{\pi_D}|\pi_2^2\rangle = \langle \pi_D|J^+_{\pi_U}|\pi_2^2\rangle = -\frac{\sqrt{6}}{12},$$

$$\langle \pi_+|\hat{J}^+_{\pi^-}|\pi_2^2\rangle = \langle \pi_-|\hat{J}^+_{\pi^+}|\pi_2^2\rangle = \frac{\sqrt{6}}{4} \quad \langle \pi_+|\hat{J}^+_{\pi^-}|\pi_1^2\rangle = \langle \pi_-|\hat{J}^+_{\pi^+}|\pi_2^2\rangle = -\frac{\sqrt{6}}{12} \tag{5}$$

Although the matrix elements involving cross-terms are negative, since π_1^2 and π_2^2 are not distinguished on the quark level, any other linear combination will also work. With the symmetric and anti-symmetric linear combination

$$|\pi_0^2\rangle = \frac{1}{2}\left(|\pi_1^2\rangle + |\pi_2^2\rangle\right), \qquad |\bar{\pi_0}^2\rangle = \frac{1}{2}\left(|\pi_1^2\rangle - |\pi_2^2\rangle\right) \tag{6}$$

we find

$$\langle \pi_U|\hat{J}^+_{\pi_D}|\pi_0^2\rangle = \langle \pi_D|\hat{J}^+_{\pi_U}|\pi_0^2\rangle = \langle \pi_+|\hat{J}^+_{\pi_-}|\pi_0^2\rangle = \langle \pi_-|\hat{J}^+_{\pi_-}|\pi_0^2\rangle = \frac{1}{2\sqrt{6}},$$

$$\langle \pi_U|\hat{J}^+_{\pi_D}|\bar{\pi_0}^2\rangle = \langle \pi_D|\hat{J}^+_{\pi_U}|\bar{\pi_0}^2\rangle = \langle \pi_+|\hat{J}^+_{\pi_-}|\bar{\pi_0}^2\rangle = \langle \pi_-|\hat{J}^+_{\pi_-}|\bar{\pi_0}^2\rangle = \frac{1}{\sqrt{6}} \tag{7}$$

All the other matrix elements can be consistently combined to result in only positive values.

3. Dependence of the chemical potential

In the static limit, which corresponds in our setup to the high temperature limit where pion exchange is absent, we have $Z = Z_1^V$ with Z_1 is 1-dim QCD partition function. All 92 states $\mathfrak{h} \in \mathbb{H}_\mathfrak{h}$ contribute with a weight that depends on the baryon and isospin chemical potential. Based on the Conrey-Farmer-Zirnbauer formula [16] we have derived Z_1 or degenerate quark mass $m \equiv m_u = m_d$, with $\mu_c = \mu_c(m)$ the effective mass as a function of the bare mass:

$$\begin{aligned} Z1\left(\frac{\mu_B}{T}, \frac{\mu_I}{T}, \frac{\mu_c}{T}\right) = {} & 2\cosh\frac{3\mu_I}{T} + 4\left(\cosh\frac{\mu_c}{T}\right)^2\left(3 + 2\cosh\frac{4\mu_c}{T} + 2\cosh\frac{2\mu_I}{T}\right) \\ & + 4\cosh\frac{\mu_I}{T}\left(2 + 2\cosh\frac{2\mu_c}{T} + \cosh\frac{4\mu_c}{T}\right) \\ & + 8\cosh\frac{\mu_B}{T}\left(2\cosh\frac{\frac{3}{2}\mu_I}{T}\cosh\frac{\mu_c}{T} + \cosh\frac{\frac{1}{2}\mu_I}{T}\left(2\cosh\frac{2\mu_c}{T} + 1\right)\right) \\ & + 2\cosh\frac{2\mu_B}{T} \end{aligned} \tag{8}$$

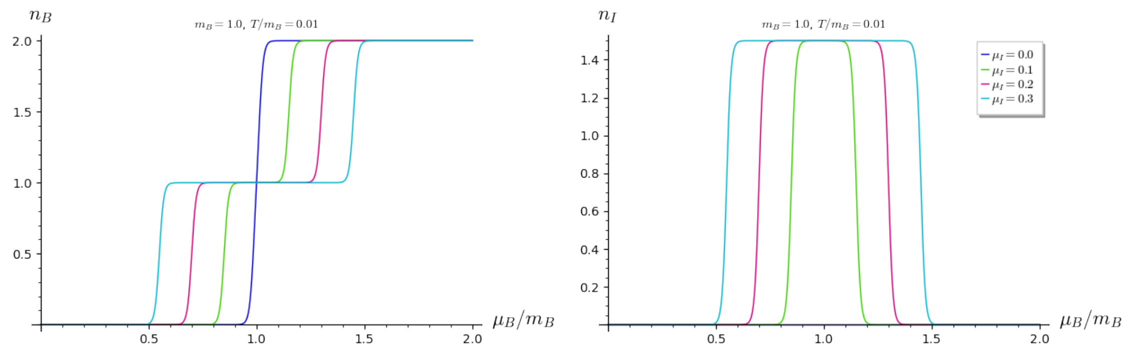

Figure 2: Result on the baryon density (left) and isospin density (right) at non-zero isospin chemical potential in the static limit (corresponding to the high temperature limit at strong coupling).

The Quantum Hamiltonian at finite quark mass still only contain 92 hadronic states per site, but a set of annihilation/creation operators on a single site need to be included, which we will discuss in a forthcoming publication. In Fig. 2 the baryon density and isospin density as obtained by taking derivatives from Eq. (8) is show for various isospin chemical potentials at fixed baryon chemical potential and temperature. We find that for $\mu_I > 0$ the baryon density n_B signals two transitions, the first taking place when the isospin density jumps to its maximal value $n_I = 3/2$, the second transition taking place when the isospin density vanishes again, which is due to Pauli saturation. A non-zero isospin density does only admits a single baryon, but not $n_B = 2$. This behaviour is consistent with $N_f = 2$ meanfield theory [5], which is based on a $1/d$ expansion for staggered fermions. Here it was found that at non-zero isospin density: two critical end-points exist, at the first transition the condensate σ_u vanishes in the second transition also σ_d vanishes. We aim to confirm this scenario with Monte Carlo simulations.

4. Setup of the Quantum Monte Carlo Simulation

The $N_f = 2$ QMC algorithm is an extension of the $N_f = 1$ QMC and is also realized as a continuous time version of the Worm algorithm for strong coupling LQCD [11]. We will focus here mainly on the modification required for $N_f = 2$:

- The initial configurations chooses for every spatial site one of the 92 states according to the values of the chemical potentials μ_B, μ_I.
- Prior to the worm updates, a specific meson Q from the four possible states $\{\pi_U, \pi_D, \pi_+, \pi_-\}$ has to be chosen randomly, and both $\hat{J}^+_Q$, $\hat{J}^-_Q$ will be fixed during worm evolution until the worm closes.
- The move update chooses a new admissible site for worm head and tail to start the Poisson process. During the Poisson process (shift updates), the worm head moves continuously in time until it emits or absorbs a spatial pion of charge Q.
- The emission ("decay") probabilities $\exp(-\lambda_Q(t)\Delta_t)$ are according to the matrix product, $\lambda \sim \hat{J}^+_{Q,x}\hat{J}^-_{Q,y}/T$ for emission from site x to site y after some time Δt, with T the temperature.

The lower the temperature, the more interactions are generated. The decay constant λ is in contrast to $N_f = 1$ not independent of the time: the number of admissible neighbors from which the site y is chosen depends on the hadronic state $\mathfrak{h}$ at t: Due to the emission/absorption of charged pions $\pi^{\pm}$, isospin may change over time at the neighboring sites.

- After the worm head and tail recombine, a static update is probed for all sites to which no spatial pion is attached: again, for those sites a new of the 92 hadronic states is chosen, which may change the baryon number (that cannot be changed during Worm evolution as baryons are static in the continuous time limit).

The baryon and isospin density can be measured on each configuration after worm update, by averaging over time slices. Also the chiral and pion susceptibilities can be obtained from the 2-point correlation functions measured during worm evolution as so-called improved estimators. Preliminary results have been obtained by scanning in baryon chemical potential at fixed isospin chemical potential and have indeed found a plateau between the two transitions that increases with increasing isospin density. As the temperature dependence still needs to be investigated, we decided not to include these results in this proceedings.

5. Summary and Outlook

We have presented an extensions to the Hamiltonian formulation of strong coupling lattice QCD from $N_f = 1$ to $N_f = 2$ and gave a detailed account of the way the hadronic states are used in a QMC algorithm. The simulations are sign-problem free. We are still in the process to map out the enlarged phase diagram in the $\mu_B - \mu_I - T$-space and will present results on the nuclear and chiral transition and pion condensation in a forthcoming publication.

We plan to extend this framework in two directions: (1) by including the effect of quark masses, and (2) by including the gauge corrections to the strong coupling limit. Whereas (1) will not alter the number of hadronic states, but will add new interactions between the hadronic states, (2) will add new quantum states which are not purely hadronic, but involve combinations of quarks and gluons as color singlets on which creation and annihilation operators act upon. It is not yet guaranteed that these extensions are sign-problem free, but it is in any case much milder than on a lattice with discrete time.

This work was supported by the Deutsche Forschungsgemeinschaft (DFG, German Research Foundation) – project number 315477589 – TRR 211.“

References

[1] Pietro Rossi and Ulli Wolff. Lattice QCD With Fermions at Strong Coupling: A Dimer System. *Nucl. Phys.*, B248:105–122, 1984.

[2] F. Karsch and K. H. Mutter. Strong Coupling QCD at Finite Baryon Number Density. *Nucl. Phys.*, B313:541–559, 1989.

[3] Philippe de Forcrand and Michael Fromm. Nuclear Physics from lattice QCD at strong coupling. *Phys. Rev. Lett.*, 104:112005, 2010.

[4] N. Kawamoto and J. Smit. Effective Lagrangian and Dynamical Symmetry Breaking in Strongly Coupled Lattice QCD. *Nucl. Phys.*, B192:100, 1981. [,556(1981)].

[5] Yusuke Nishida. Phase structures of strong coupling lattice QCD with finite baryon and isospin density. *Phys. Rev.*, D69:094501, 2004.

[6] Giuseppe Gagliardi and Wolfgang Unger. New dual representation for staggered lattice QCD. *Phys. Rev. D*, 101(3):034509, 2020.

[7] Philippe de Forcrand, Jens Langelage, Owe Philipsen, and Wolfgang Unger. Lattice QCD Phase Diagram In and Away from the Strong Coupling Limit. *Phys. Rev. Lett.*, 113(15):152002, 2014.

[8] J. Kim, O. Philipsen and W. Unger, PoS **LATTICE2019** (2019), 064 doi:10.22323/1.363.0064 [arXiv:1912.00822 [hep-lat]].

[9] J. Kim and W. Unger, PoS **LATTICE2016** (2016), 035 doi:10.22323/1.256.0035 [arXiv:1611.09120 [hep-lat]].

[10] Philippe de Forcrand, Wolfgang Unger, and Helvio Vairinhos. Strong-Coupling Lattice QCD on Anisotropic Lattices. *Phys. Rev.*, D97(3):034512, 2018.

[11] Marc Klegrewe and Wolfgang Unger. Strong Coupling Lattice QCD in the Continuous Time Limit. *Phys. Rev. D*, 102(3):034505, 2020.

[12] John B. Kogut and Leonard Susskind. Hamiltonian Formulation of Wilson's Lattice Gauge Theories. *Phys. Rev. D*, 11:395–408, 1975.

[13] Neven Bilic, Frithjof Karsch, and Krzysztof Redlich. Flavor dependence of the chiral phase transition in strong coupling QCD. *Phys. Rev.*, D45:3228–3236, 1992.

[14] W. Unger and P. Pattanaik, PoS **LATTICE2021** (2022), 597 doi:10.22323/1.396.0597 [arXiv:2112.11875 [hep-lat]].

[15] K. E. Eriksson, N. Svartholm, and B. S. Skagerstam. On Invariant Group Integrals in Lattice QCD. *J. Math. Phys.*, 22:2276, 1981.

[16] L. Ravagli and J. J. M. Verbaarschot, Phys. Rev. D **76** (2007), 054506 doi:10.1103/PhysRevD.76.054506 [arXiv:0704.1111 [hep-th]].